

Blending from binarity in microlensing searches towards the Large Magellanic Cloud

T. Blaineau¹, M. Moniez¹

Laboratoire de physique des 2 infinis Irène Joliot-Curie, CNRS Université Paris-Saclay, Bât. 100, Faculté des sciences, F-91405 Orsay Cedex, France

Received 06/03/2023, accepted 06/03/2023

ABSTRACT

Context. Studies of gravitational microlensing effects require the estimation of their detection efficiency, as soon as one wants to quantify the massive compact objects along the line of sight of source targets. This is particularly important for setting limits on the contribution of massive compact objects to the Galactic halo. These estimates of detection efficiency must not only account for the blending effects of accidentally superimposed sources in crowded fields, but also for possible mixing of light from stars belonging to multiple gravitationally bound stellar systems.

Aims. Until now, only accidental blending have been studied, in particular thanks to high resolution space images. We address in this paper the impact of unresolved binary sources in the case of microlensing detection efficiencies towards the Large Magellanic Cloud (LMC).

Methods. We use the Gaia catalog of nearby stars to constrain the local binarity rate, which we extrapolate to the distance of the LMC. Then, we estimate the maximum fraction of the cases for which a microlensing event could be significantly modified, as a function of the lens mass.

Results. We find that less than 6.2% of microlensing events on LMC sources due to halo lenses heavier than $30M_{\odot}$ can be significantly affected by the fact that the sources belong to unresolved binary systems. For events caused by lighter lenses on LMC sources, our study shows that the risk of blending effects by binary systems is likely to be higher and efficiency calculations remain more uncertain.

Key words. Gravitational lensing: micro - Cosmology: dark matter - surveys - stars: binaries - Galaxy: halo - Galaxy: kinematics and dynamics

1. Introduction

Objects catalogued in dense fields are frequently composed of several blended sources. Ignoring this fact may distort the statistical conclusions of the microlensing searches because of its impact on detection efficiency. Some of the consequences of blending on microlensing have been studied by comparing ground-based images with high-resolution deep space images obtained notably with the Hubble Space Telescope (HST) (HST archive 2002). These space images allow to quantify the impact of accidental superpositions of sources in the catalogs of the ground-based surveys, due to the high density of the field (Tisserand et al. 2007; Wyrzykowski et al. 2011). However, another component of the blending remains poorly understood, that resulting from the mixing of light from multiple gravitationally bound stars. Space telescopes themselves are unable to resolve such systems when they are at a distance as large as the Large Magellanic Cloud (LMC). Their existence is an additional cause of blending, distinct from the mixing caused by coincidental alignments. In this paper we study the consequences, currently poorly known, of the binarity of stars on the detectability of the gravitational microlensing effects they may experience. In particular,

we will study the case of the detection efficiency of microlensing effects due to high mass ($> 30M_{\odot}$) Galactic halo objects, which have been recently searched in the LMC direction and excluded as a significant component of the hidden mass of the Galaxy (Blaineau et al. 2022). In section 2, we recall the fundamentals of the gravitational microlensing effect. In Section 3 we introduce the blending effects and their impact on the detection efficiency. We introduce the case of multiple sources and distinguish between three blending regimes. In section 4, we present our statistical analysis tools and show that we cannot extract statistical information on the LMC binary systems from HST images because of the separation limit. In section 5, we describe our methodology to estimate upper values of the local system binarity rate. We show how the distribution of distances between the components of star pairs in a complete GAIA catalog population allows us to quantify the rate of widely separated double systems in the Galactic plane. We extrapolate the local binarity rate down to $50AU$ separations for stars closer than $500pc$ to the Sun in section 6. In section 7, we quantify the maximum impact of binarity on the microlensing detection efficiency towards the LMC as a function of the projected lens Einstein radius. We discuss the validity domain and limitations of our study, and address the question of the dependence of binarity rates on the stellar type in

Send offprint requests to: M. Moniez,
e-mail: moniez@1a1.in2p3.fr

Section 8. We conclude and summarize our results in Section 9, and propose some prospects for future microlensing surveys.

2. Overview of microlensing

2.1. Description of a microlensing event

The gravitational microlensing effect (Paczynski 1986), first discovered in 1993 (Alcock et al. 1993; Aubourg et al. 1993; Udalski et al. 1993), occurs when a massive compact object (the lens) passes close enough to the line of sight of a background source and temporarily magnifies its brightness. Reviews of the microlensing formalism can be found in Schneider et al. (2006) and Rahvar (2015). When a single point lens of mass M_L located at distance D_L deflects the light from a point source located at distance D_S , a situation hereafter called PSPL event, an observer receives light from two images not separated in the telescopes. The total magnification $A(t)$ of the apparent luminosity of the source is given by (Paczynski 1986):

$$A(t) = \frac{u(t)^2 + 2}{u(t) \sqrt{u(t)^2 + 4}}, \quad (1)$$

where $u(t)$ is the distance of the lens to the undeflected line of sight, divided by the Einstein radius r_E ,

$$r_E = \sqrt{\frac{4GM_L}{c^2} D_S x(1-x)} \approx 4.5 \text{ AU} \left[\frac{M_L}{M_\odot} \right]^{\frac{1}{2}} \left[\frac{D_S}{10 \text{ kpc}} \right]^{\frac{1}{2}} \frac{[x(1-x)]^{\frac{1}{2}}}{0.5}. \quad (2)$$

G is the Newtonian gravitational constant, and

$$x = D_L/D_S. \quad (3)$$

If the point lens has a constant relative transverse velocity v_T with respect to the point source (PSPL *rectilinear* event), and $u(t)$ reaches its minimum value u_0 (impact parameter) at instant t_0 , then

$$u(t) = \sqrt{u_0^2 + (t - t_0)^2/t_E^2}, \quad (4)$$

where $t_E = r_E/v_T$ is the lensing timescale,

$$t_E \sim 79 \text{ days} \times \left[\frac{v_T}{100 \text{ km/s}} \right]^{-1} \left[\frac{M_L}{M_\odot} \right]^{\frac{1}{2}} \left[\frac{D_S}{10 \text{ kpc}} \right]^{\frac{1}{2}} \frac{[x(1-x)]^{\frac{1}{2}}}{0.5}. \quad (5)$$

In the case of the study of a population of stellar sources within the LMC, and assuming that independently of their mass the lenses are distributed in a spherical, isotropic and isothermal halo with the density distribution described in Griest (1991) and with the parameters used in Blaineau et al. (2022) (hereafter called standard halo), the average duration of the events due to the lenses of a given mass M_L is $\langle t_E \rangle \sim 63 \text{ day} \sqrt{M_L/M_\odot}$.

2.2. Optical depth, event rate, detection efficiency

The microlensing optical depth τ is defined as the probability that the line of sight to a source is within one r_E of a lens (corresponding to $A_{max} > 1.34$ according to Eq. (1)) The event rate is the number of microlensing events per star per unit time with $u_0 < 1$. This rate is related to the optical depth by the following relation: $\Gamma = (2/\pi)\tau/\langle t_E \rangle$ (Griest 1991). The event rate is estimated from the duration distribution of the observed events, and must take into account the observational average detection

efficiency that depends a priori on the time sampling, the photometric accuracy, the source population, the background noise and the search algorithm. The probability to detect a given event depends on the parameters of this event (u_0 , t_0 , t_E , source magnitude), and the efficiency $\epsilon(t_E)$ is defined as the ratio between the following two numbers: The numerator is the sum of the detection probabilities of all events with *measured* duration t_E and *measured* $u_0 < 1$ (whatever their other parameters), and the denominator is the total number of expected events with *true* duration t_E , *true* $u_0 < 1$, and *true* t_0 within the survey duration. This efficiency is usually calculated by Monte Carlo simulation of microlensing events, combined with observed light curves of stable stars to produce realistic light curves of microlensing events, and then subjected to the same analysis as the real data.

Basic Monte-Carlo efficiency estimates assume that the events are of the PSPL rectilinear type, *i.e.* that the magnification curve is given by the equations (1) and (4). Concerning the studies towards the LMC, it has been established that the contribution of the events that could escape detection due to lens binarity does not exceed 10% (Mróz et al. 2019); the impact of the parallax effects (due to the orbital motion of the Earth around the Sun), which distort the magnification curve, is also negligible towards the LMC (Blaineau & Moniez 2020). The subject of this paper is to explore the impact of blending on the efficiency, taking into account not only the blending of accidentally aligned sources already discussed in several works (see for example Tisserand et al. (2007) and Wyrzykowski et al. (2011)), but also the contribution of multiple gravitationally bound stellar systems.

3. Blending effects in microlensing searches: the unknown contribution of binary stars

Blending affects the efficiency of a microlensing search in several ways. On the one hand, the fact that a cataloged object is made up of light from several unresolved stars must be taken into account when estimating the effective number of stars monitored. A microlensing event can indeed occur on each of the stars composing the cataloged source, increasing the number of stars actually susceptible to lensing compared to the number of sources counted in the catalog. On the other hand, the light contribution of other stars modifies the shape of the observed light curve from a microlensing event, in a variable way depending on the color. The efficiency of the search algorithms can then be affected by the following effects:

- The shape of the light curve can no longer be exactly fitted by that of a simple (PSPL) event, which can cause events to be missed if blending is ignored.
- As soon as the blend is composed of stars of different colors, the apparent magnification is no longer achromatic: this can reduce the efficiency of a search algorithm that considers only achromatic events.
- The apparent maximum magnification is smaller than the maximum magnification of the lensed star; therefore the measured (or apparent) impact parameter u_0 is larger than the physical (true) impact parameter.
- The apparent Einstein duration t_E estimated by fitting the light curve of a blended event with the curve of a PSPL event is systematically shorter than its real value. This means that, since the efficiency of the analysis depends on the measured duration of the event, there is also a modification of the expected number of events as a function of the duration.

All these effects impact the number of expected events in a non-trivial way and can potentially modify it, so it is necessary to

properly take into account this blending effect for the interpretation of microlensing effect searches, especially to evaluate the optical depths. As mentioned above, the confusion of several stars in a single cataloged object has several possible origins: the superposition may be due to an accidental coincidence (accidental blending), depending on the field crowding, or it may be due to the existence of binary or multiple systems (binary blending). The estimation of accidental blending as it is classically obtained, makes the assumption of a locally uniform density distribution of stars; on the other hand the impact of superposition due to multiple systems, the binary blending, cannot be estimated in the same way.

Considering the case of two stars blended into a single cataloged object, we distinguish three blending regimes depending on their separation:

- As long as the angular separation δ between the two stars is large compared to both angular Einstein radii of the lens configurations¹, we can consider them as independent in the context of the calculation of the expected number of events: we are in a blending regime that we can consider as classical or ordinary, since it is the one that occurs almost exclusively in the case of accidental mixing, and we observe then the addition of a constant flux to an amplified flux. Previous studies have shown that the impact of this blending regime is small (< 10%) and positive on the detection efficiency (Blaineau et al. (2022) and references included).
- If the angular separation δ between the two stars is small compared to the angular Einstein radii of both lens configurations, then both components undergo the same apparent magnification simultaneously, and everything happens as if a single star of flux equal to the sum of the two stellar fluxes undergoes a PSPL microlensing effect, as in the absence of blending. According to simple geometrical considerations, this regime has a negligible probability of occurring for accidental blending, but not in the case of blending due to binarity. In the latter case, the Einstein radii are identical for the microlensing of both stars.
- If the angular separation δ between the two stars is of the order of the angular Einstein radii of both lens configurations, then we are in an intermediate regime, where the light curve can be described neither by a PSPL microlensing effect nor by the addition of a constant flux to an amplified flux. In this case, we observe the superposition of two events, with different magnifications, and maxima shifted in time. Depending on the geometrical configuration, two clearly separated peaks or a single asymmetric peak may appear. Several examples of magnification curves are shown in Fig. 1, with the corresponding geometrical configurations of sources and deflectors. As with the previous regime, this situation can occur only in the case of blending due to binarity, and the Einstein radii are identical for the microlensing of both stars.

To quantify the impact of multiple sources on microlensing toward the LMC, we first need a way to count them. The following section shows why the limitations of space-based observations towards the LMC lead us to study a population of the solar environment using Gaia data (Gaia Collaboration et al. 2016).

¹ If the two stars are not at the same distance D_L , then the Einstein rings for microlensing by the same given lens are different.

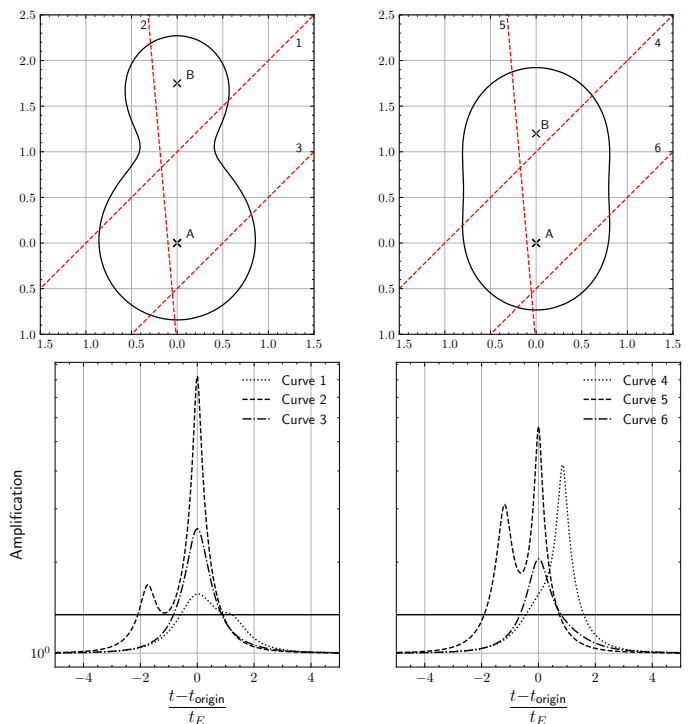


Fig. 1: (up) Three different trajectories of a deflector (red dashed) in front of two stars A and B blended into a single cataloged source; on the left stars A and B share 80% and 20% of the total luminous flux, on the right both stars have the same luminosity. The black outline corresponds to the positions where the deflector must be for the source-system to undergo a total magnification of 1.34. The coordinates are in units of Einstein radius, which is the same for both stars (located at the same distance).

(down) Magnification curves of the cataloged source-system corresponding to the trajectories above, travelled from left to right. The black line corresponds to a magnification of 1.34. t_{origin} is the time when the deflector is closest to the star A (and thus does not always coincide with the time of maximum apparent amplification). Curves 3 and 6 are very close to microlensing curves with ordinary blending because the deflector passes far from star B.

4. Angular and physical distance separation between LMC stars detected by HST

The spatial distribution of LMC stars is not expected to be uniform if it includes multiple bound systems. This is why we work with the distribution of the number of pairs of stars as a function of their separation (angular or spatial) and the two-point angular correlation function. The correlation function is calculated with the Landy-Szalay estimator (Landy & Szalay 1993), which compares the number of pairs in the data with the number of pairs in a simulation of a uniform spatial distribution in the same spatial domain. The other way to study multiple systems is to count the number of pairs as a function of their angular separation δ . We expect this distribution to be the sum of a contribution due to fortuitous alignments and an excess at the smallest values of δ if there are multiple gravitationally bound systems in the set of the pairs. From simple geometrical considerations, the first contribution is a distribution which increases linearly with δ as long as δ is small enough so that edge effects do not limit the catalog used.

The second contribution, when it exists, is expected for smaller values of δ .

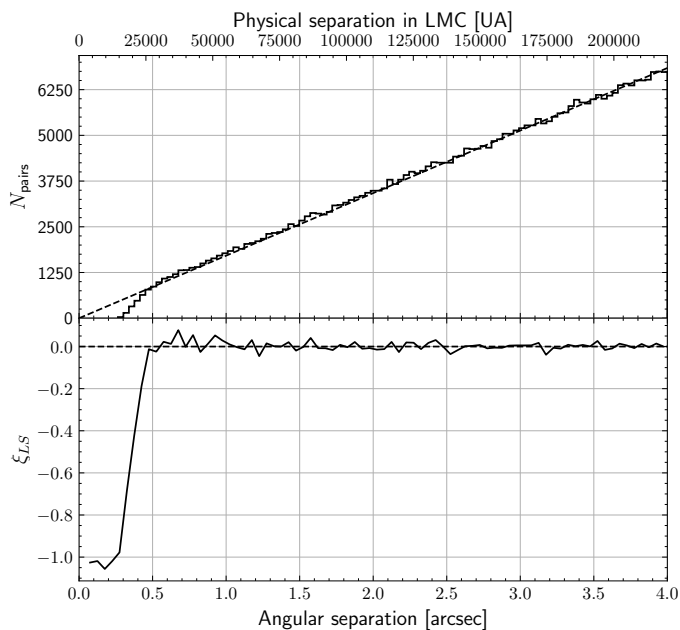


Fig. 2: (up) Number of pairs of stars per 1.2 arcsec interval as a function of their angular separation in a HST crowded LMC field image. The dotted line gives the predicted distribution of angular separations in the case of a spatially uniform distribution of stars with the same average star density.

(Down) The measured two-point angular correlation function of the detected stars in the same field.

The lower scale is the angular separation δ and the upper scale gives the corresponding transverse separation in the LMC.

Figure 2 shows the distribution of the number of pairs (up) and the two point correlation function (down), as a function of the angular separation δ of the stars detected by SExtractor algorithm (Bertin & Arnouts 1996) on an image of a crowded field of the LMC. This image has been obtained by coadding the images taken with the f555w and f814w filters by the Wide Field Planetary Camera 2 (WFPC2) of HST² (HST archive 2002). We notice that the correlation function remains zero down to the HST resolution limit (about $0.5''$), decreases below $0.5''$ and is -1 below $0.25''$, which indicates that the algorithm can never distinguish two stars separated by less than $0.25''$. Since there is no positive correlation for small separations, this shows that we also do not detect an excess of pairs in the HST data over a random distribution beyond a separation of $0.5''$, which corresponds to a transverse separation of $27500AU$ in the LMC. This situation is not surprising, since gravitationally bound systems at such distances are very rare (Dhital et al. 2010; Duchêne & Kraus 2013). The LMC is therefore too far away for HST to resolve multiple systems that would cause a significant excess of close pairs compared to a random spatial distribution.

² HST images `hst_08676_08_wfpc2_f555w_wf` and `hst_08676_08_wfpc2_f814w_wf`, at (RA, Dec) = (05h06m35.18s, -69°20'45.6'').

5. How to constrain the binarity rate in the LMC?

Since the LMC is too far away, we studied a stellar population close to us, using data from the Gaia mission, and then we extrapolate the results to the distance of the LMC. First, we define the binarity rate we will use and describe our estimation method based on star pair counts.

5.1. Methodology

We wish to know the proportion of LMC objects in EROS or MACHO type catalogs that are binary systems as a function of their transverse separation a_t . As we have just seen, the LMC is too far away for even space missions to resolve such systems. We therefore study a population of nearby stars cataloged by Gaia, for which the resolution of systems is possible as soon as $a_t > 500AU$. In the following, we call *object* an element of the Gaia catalog (that can be made of a single star or more complex system) and we call *system* a cluster of objects that we consider as gravitationally bound system (typically a resolved binary system). We will then count the binary stars in the local space, in a situation where they are well separated. Let's define n_{tot}^* as the total number of *objects* in the catalog, and $n_{bin}^*(a_t)$ as the number of objects belonging to a resolved binary *system* (i.e. made of two cataloged object), with a transverse separation $> a_t$. From these simple counts of the resolved double star systems, we can numerically compute the function:

$$f_{bin}(a_t) = \frac{1}{n_{tot}^*} \frac{dn_{bin}^*(a_t)}{da_t}. \quad (6)$$

$f_{bin}(a_t)$ is the differential probability that a Gaia cataloged *object* belongs to a double *system* separated by a projected distance a_t . This is a function that we will directly derive from the Gaia catalog in the next sections. We then define $F_{bin}(a_t)$, the integrated *system* binarity rate, as the ratio between the number of binary *systems* (unlike objects) with transverse separation $> a_t$, to the total number of *systems* :

$$F_{bin}(a_t) = \frac{n_{bin}^*(a_t)/2}{(n_{tot}^* - n_{bin}^*) + n_{bin}^*/2} = \frac{n_{bin}^*(a_t)/n_{tot}^*}{2 - n_{bin}^*/n_{tot}^*}. \quad (7)$$

Note that the total number of *systems* at the denominator corresponds to the sum of the single star systems plus all the resolved binary systems –not only the systems separated by more than a_t –³. From the definition of $f_{bin}(a_t)$ we obtain

$$\frac{n_{bin}^*(a_t)}{n_{tot}^*} = \int_{a_t}^{\infty} f_{bin}(a) da, \quad (8)$$

which is the fraction of *objects* belonging to a binary *system* with transverse separation $> a_t$. n_{bin}^* is the total number of *objects* belonging to a binary *system* resolved by Gaia (depending on Gaia's resolution power). This number is estimated from

$$\frac{n_{bin}^*}{n_{tot}^*} = \int_{a_t^{resol}}^{\infty} f_{bin}(a_t) da_t, \quad (9)$$

where a_t^{resol} is the separation limit of Gaia in the catalog we use. As Gaia's resolution is not a step function, we start integrating from a very small separation $a_t^{resol} = 50AU$, below which we are sure Gaia cannot separate 2 components, but to which we

³ As no binary system is resolved in the LMC, we will need to use this definition of a rate relative to the systems, instead of a rate relative to the –unknown– underlying number of stars.

will extrapolate our measurements in Section 6. This conservative choice then gives us a lower bound on n_{bin}^* , and thus an upper bound on F_{bin} in the equation (7). This choice is not critical, since we will show that the integral (9) is much smaller than 2, and has therefore a minor impact in the denominator of Eq. (7).

5.2. Binarity of stars closer than 600pc in the GAIA-EDR3 catalog

We have used the Gaia-EDR3 catalog (Gaia Collaboration et al. 2020) for a preliminary assessment of the impact of binarity in microlensing studies. This exploratory work does not aim to extract binarity rates, but rather upper limits on the amount of multiple source systems that can give rise to complex gravitational microlensing effects. Our immediate goal is therefore to estimate the maximum fraction of binary systems separated by transverse (or projected) distances a_t comparable to or larger than the Einstein radius of a possible lens.

In our definitions of the binarity rate, we have neglected the contribution of stellar systems made of more than two stars, since we find only 1% of such systems with angular size smaller than $10''$ (corresponding to $a_t < 6000AU$ at $600pc$ distance) in the selection of stars defined in the next paragraph. We will therefore neglect this type of system in our treatment of blending effects. The estimate of the transverse (or projected) physical distance a_t of two stars in the Gaia catalog is deduced from the angular distance δ between the two components and their annual parallax measurements π (in ArcSec), assuming that they both have an intrinsic uniform and rectilinear motion⁴ (Lindergren et al. 2012, 2021), by $a_t = 1AU \times \delta/\pi$. The parallax differences between components being too imprecise compared to the angular accuracies, we cannot make a study in the 3 dimensions which would include the longitudinal distance (along the line of sight). In the following analysis, parallaxes are just used to convert angular distances into transverse distances and also to reduce the risks of association of very distant objects, accidentally located on the same line of sight, by considering only pairs of stars with compatible parallaxes.

We selected the stars of the Gaia-EDR3 catalog (Gaia Collaboration et al. 2020), whose apparent magnitude is $3 < g < 18$, a domain in which the catalog is complete (thus not biased) (Fabricius et al. 2020). Then we limited our sample to stars closer than 600pc (corresponding to a parallax $\pi > 1.66mas$). At this distance, a separation of $1''$ corresponds to $600AU$. We also require that the parallax accuracy be better than 20%. The bias (Luri et al. 2018) induced by this selection can be neglected because we reject only 2% of the stars, the most distant of our sample. Finally, we have restricted our study to Galactic latitudes higher than 20° to avoid the very crowded and inhomogeneous areas of the Galactic plane (figure 3).

Figure 4 shows the distribution of the absolute magnitude G of the stars of the GAIA catalog closer than 600pc, as a function of their distance estimated by their parallax. This catalog is complete between the lines of equal apparent magnitude marked by the thick red curves ($g = 3$ and $g = 18$). We define 5 shells (Fig. 3 and 4), delimited by the spheres of radii (50, 140, 230, 320,

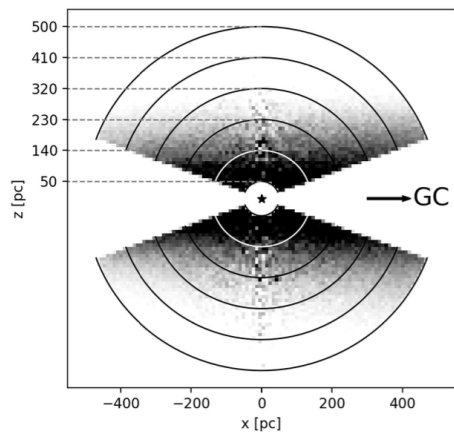


Fig. 3: Projection perpendicular to the Galactic plane of the spatial distribution of the stars of the Gaia catalog, and representation of the limits of the shells used in our study. The representation is centered on the Sun.

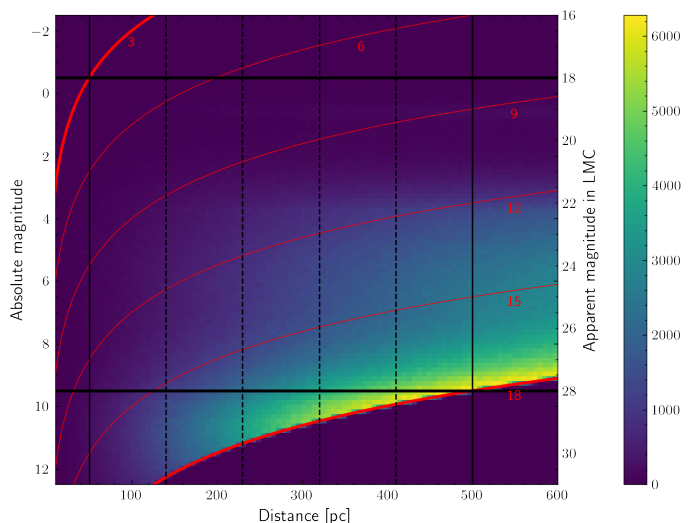


Fig. 4: Distribution of the number of stars in Gaia EDR3 as a function of their distance and absolute magnitude (left scale). The right scale gives the apparent magnitude that these stars would have in the LMC. Gaia catalog is complete between the thick red curves. The red lines are the iso-apparent-magnitude lines in Gaia in the (Distance, absolute magnitude) plane. We restrict the study to stars within the absolute magnitude range delimited by the thick horizontal black lines ($-0.5 < G < 9.5$), which ensures homogeneity of stellar type over the volume we consider; the vertical solid lines correspond to the distance limits of our sample. The vertical dashed black lines delineate the distance domains of the shells we will consider in our analysis (between 50 and 500pc).

410 and 500pc) and study separately the pairs of stars in each shell (Table 1).

These subdivisions allow us to verify that the separation distributions of the binaries are indeed functions of the physical distances a_t , independently of the angular distances δ , as long as these are greater than the separation power of Gaia. To ensure that the distributions studied in the 5 shells considered are all complete, we only study the stellar population whose absolute

⁴ Since we are trying to quantify binary systems, we must remember that the rotation of the stars of a system around the center of gravity alters the uniform rectilinear motion assumed in the estimation of parallaxes. As we are only interested in binary systems separated by more than $50AU$, with orbital periods of the order of a few centuries, we can consider that the variation of orbital velocity on the apparent trajectory of the stars on the sky has only a negligible impact on the estimation of parallaxes in Gaia.

| shell limits | a_t for $\delta = 2''$ separation | number of stars in shell | effective |
|--------------|--|-----------------------------|-----------|
| [50-140] pc | [100-280]AU | 160409 | 158000 |
| [140-230] pc | [280-460]AU | 481496 | 465000 |
| [230-320] pc | [460-640]AU | 867259 | 807000 |
| [320-410] pc | [640-820]AU | 1259719 | 1109000 |
| [410-500] pc | [820-1000]AU | 1634717 | 1313000 |

Table 1: Limits and contents of the shells (see text).

magnitude is in the range $-0.5 < G < 9.5$ (between the thick black lines in Figure 4). Finally, we only consider pairs of stars with a magnitude difference of less than 2.5, beyond which we can neglect the impact of the less luminous component on the light curve of a microlensing effect.

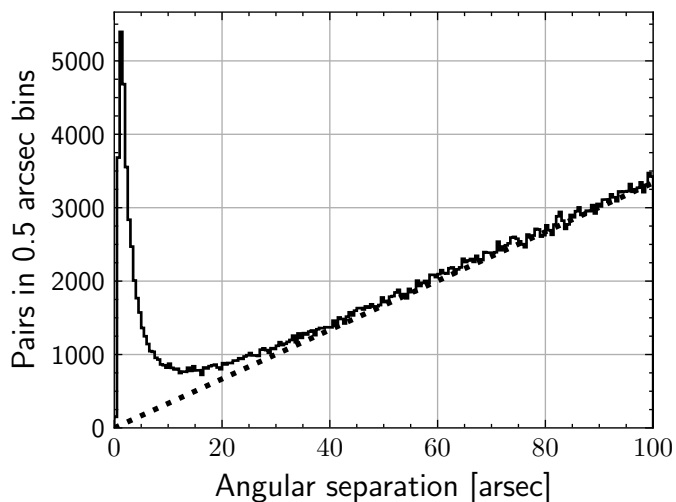


Fig. 5: Number of star pairs per 0.5 arcsec interval as a function of their angular separation. The dotted line gives the predicted distribution in the case of a spatially uniform distribution with the same average star density. Only stars with Galactic latitude larger than 60° are considered here (1,233,947 stars). We measure about 29,000 pairs in excess of accidental pairs.

Figure 5 shows the angular separation distribution δ for the pairs of stars closer than $600pc$. We first observe a clear excess of pairs for $\delta < 20''$, in agreement with Zavada & Píška (2020), which demonstrates the existence of Gaia-detectable bound systems within $600pc$, in contrast to the situation in Fig. 2 which showed the inability of HST to separate bound systems in the LMC. Second, we note that like HST, our algorithm fails to separate stars that are too close in angular distance, in this case around $0.5''$. The question of the separation limit, as it also relates to Gaia’s scanning law, is beyond the scope of this paper (see Blaineau (2021) for more details). For our study, it is sufficient to know that we decided to focus only on pairs separated by at least $2''$ in order not to be limited by the resolution of Gaia. We have shown that the results of the next sections vary by less than 2% (half of the estimated uncertainty) if we change this minimal separation in the range $[1.5'' - 2.5'']$ (Blaineau 2021).

To estimate the binarity rate of stars in a shell, we first build the distribution of the type shown in Figure 5; then, we calculate the number of pairs remaining after subtracting the compo-

nent due to accidental alignments, as a function of the separation. This expected random component is a linear function, fitted between $60''^5$ and $120''$ (dashed line in Figure 5). Once the angular separation is converted to physical transverse separation a_t (by using the measured parallax π), from the excess in each channel of a_t we can derive an estimate of the differential stellar binarity rate $f_{bin}(a_t)$ defined by expression (6), plotted in Figure 6 for each shell. We recall that this quantity represents the differential fraction of stars in pairs *in excess* of the expected number of accidental pairs separated by a_t , per unit of a_t .

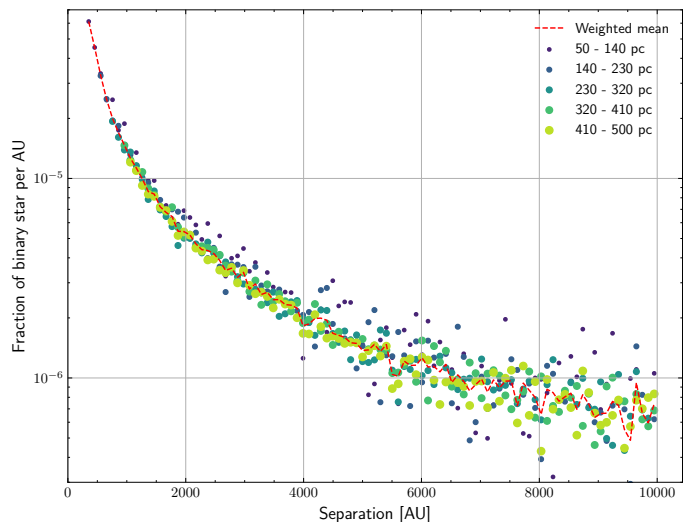


Fig. 6: Differential rate of binaries $f_{bin}(a_t)$ measured in the five shells as a function of transverse separation a_t . The red dashed line gives the means for all shells. Error bars are not shown to avoid overloading the figure, but the scatter of each series gives an indication.

The figure shows that the rates found do not depend on the shell considered, which allows us to use the average distribution, weighted by the effective number of stars in each shell; these effective numbers are the numbers of stars found within the intervals of parallax of each shell, statistically corrected for misattributions of pairs in the shells, due to uncertainties in the measured parallaxes⁶ (see also Table 1). It should be noted that the closest shells are obviously those that allow us to estimate the binarity rate at the smallest separations a_t , but at the expense of the statistics limited by the small volume of the shell. For shells at larger distances, the statistic is more comfortable, but our angular separation limit of $2''$ prevents estimates at the smallest physical separations.

6. Estimation of the local stellar binarity rate

In this section, we fit and extrapolate the differential binarity rate down to $50AU$ transverse separations.

⁵ Two stars at $\sim 450pc$ separated by $60''$ would be separated by only $0.5''$ if they were in the LMC. This directly illustrates the fact that an excess count of pair in LMC is only expected for separations much smaller than the resolution limit of HST.

⁶ These uncertainties result in uncertainties on the distance of the stars; a pair can then be either misattributed if both components are effectively in another shell, or it can be missed, if only one of the components is in another shell.

Following Duquennoy & Mayor (1991) and Raghavan et al. (2010), we considered a log-normal model for the distribution of semi-major axes a of binary systems. Since we measure projected separations a_t and not semi-major axes, this distribution is modified as follows, by considering that the orbits have no preferred inclination:

$$f_{bin}^{DM}(a_t) = A \int_{a_t}^{+\infty} \frac{a_t}{r^2 \sigma \sqrt{2\pi(r^2 - a_t^2)}} \exp\left[-\frac{(\ln r/r_{mode} - \sigma)^2}{2\sigma^2}\right] dr, \quad (10)$$

where A and σ are fitted to our data once r_{mode} is chosen, corresponding to the maximum of the distribution. If we chose $r_{mode} =$

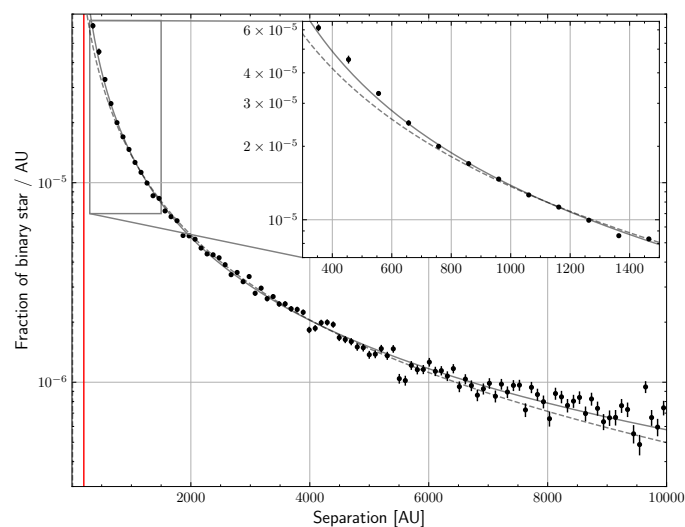


Fig. 7: Projected log-normal function f_{bin}^{DM} for $r_{mode} = 0.1AU$ (dotted line), and power function f_{bin}^{PL} (full line), fitted to the differential fraction of binary, as a function of the projected separation. The vertical red line corresponds to a projected separation of 200 AU. The inset shows that the fit of f_{bin}^{DM} is not satisfactory at small separations.

0.1AU, then we find $A = 0.126$ and $\sigma = 2.72$, but the fit is unsatisfactory for $a_t < 600AU$, and this whatever the parameter r_{mode} (Figure 7). This poor agreement can probably be attributed to the fact that this lognormal distribution was established for solar-type stars, while we study a different and more extended population. Nevertheless, following this fitted model, we compute the binarity rate for systems with $a_t > 200AU$ ⁷ using Eqs (9), then (8) and (7), and find $F_{bin}(200AU) = 2.76 \pm 0.03\%$. By varying the r_{mode} parameter within $10^{-4}AU < r_{mode} < 10^2AU$, we find values close to, contained within $2.05\% < F_{bin}(200AU) < 2.8\%$. Similarly, we find that $F_{bin}(100AU) < 3.6\%$ regardless of the r_{mode} parameter.

We also fitted to our measurements the following empirical power-law parameterization :

$$f_{bin}^{PL}(a_t) = (0.19AU^{-1}) \times (a_t/1AU)^{-1.379}, \quad (11)$$

⁷ This length corresponds to the most likely projected Einstein radius (at the LMC) of a $\sim 50M_{\odot}$ Galactic halo lens magnifying light from a LMC source.

that better describes our data for small a_t values. (Figure 7). With this alternative model for the distribution of projected separations of binaries, we find that $F_{bin}(200AU) = 3.48 \pm 0.03\%$, a value close to the one found with the previous model.

In section 5, we mentioned that the total probability of a Gaia object being a member of a resolved binary system is less than the value given by expression (9). The value we find by integrating the Eq. (11) from $a_t = 50AU$ is 0.114, which is an upper limit of the fraction of Gaia objects belonging to binaries resolved in our sample. This number is indeed small compared to 2, and its exact value does not impact the computation of F_{bin} from Eq. (7) especially since we are interested in the upper limit. It should be noted further that nothing can be said from our data about the binarity rate for $a_t < 50AU$, because extrapolation below this value is not constrained.

7. Extrapolation at the LMC; impact of binarity on microlensing detection

The previous study concerns a population of Milky Way stars with $-0.5 < G < 9.5$. In the LMC, they would have an apparent magnitude $18 < g < 28$, *i.e.*, would be among the faintest stars in a classical catalog searching for gravitational microlensing effects. This is a limitation of this work, in addition to the fact that we assume that this population has the same binarity statistical characteristics in the LMC as in the Milky Way disk.

We saw in section 3 that if the angular separation of the components of a blend is much smaller than the angular Einstein radius—expressed by $a_t \ll R_E/x$, where x is given by Eq. (3)—, then both sources undergo roughly the same magnification and everything happens as if there were only one source. It is therefore the pairs with $a_t \geq R_E/x$ whose proportion we need to estimate, to quantify their impact on the statistics of microlensing effects. From the $f_{bin}^{PL}(a_t)$ function of the differential binarity rate and using Eq. (7), we can estimate the maximum proportion of situations where binarity can significantly affect microlensing effects. Figure 8 shows this proportion as a function of R_E/x , the Einstein radius projected in the LMC, after integration over the distribution of a_t under 3 different assumptions: assuming that the blend effect is significant as soon as $a_t > R_E/2x$ (thus integrating the differential distribution from $R_E/2x$ to infinity), or only when $a_t > R_E/x$, or weighting the differential distribution between 0 and 1 (ramping) when a_t varies from $0.1R_E/x$ to $1.75R_E/x$. The latter assumption is derived from the study of Griest & Hu (1992), which discusses in detail the distortions expected by a microlensing curve for a composite source. Figure 8 shows for example that under the most pessimistic assumption (blending effect to be taken into account as soon as $a_t > R_E/2x$), less than 7% of the sources are binary systems with a luminosity difference of less than 2.5 magnitude between components, which can significantly affect the light curves of microlensing events when $R_E/x > 50AU$.

8. Discussion

8.1. Field of application

One must first remember the limitations of this work: only the population of stars of absolute magnitude $-0.5 < g < 9.5$ could be well studied, and any use for another population is an extrapolation, either for an identical population but in another galaxy with possibly different metallicity, or for a stellar population in the Milky Way with more extensive types.

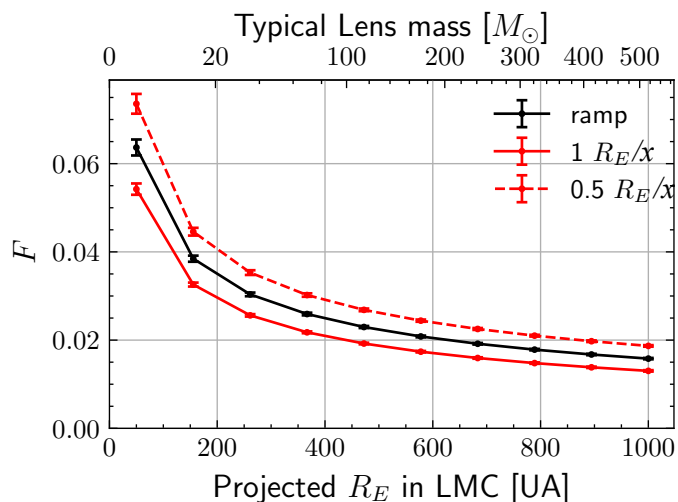


Fig. 8: Rates of binarity F_{bin} that can produce significantly distorted events as a function of the projected Einstein radius of the lens R_E/x , obtained for different ways of integration: from R_E/x (solid red), from $R_E/2x$ (dashed red), and by weighting the contributions by a ramp function (black) (see text). Typical masses corresponding to the Einstein radii are plotted on the upper abscissa for sources within the LMC.

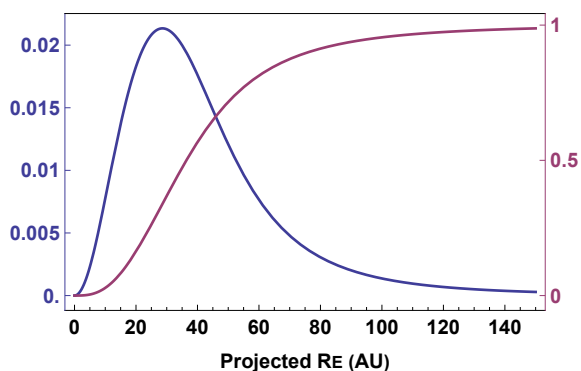


Fig. 9: Blue line: distribution of the projected Einstein radius $R_E/x = R_E D_S / D_L$ for the microlensing events towards LMC due to $1M_\odot$ lenses within the standard Galactic halo. The distribution expected for other lens masses M_L is obtained by scaling the abscissa by the factor $\sqrt{M_L/M_\odot}$. Purple line: the cumulative distribution. The most probable value of R_E/x is 28.6AU, the mean is 44.0AU, and the median is 36.5AU.

To compute the fraction of potentially complex events due to binarity as a function of the lens mass, we combine the rates from Fig. 8 with the projected Einstein radius R_E/x distribution expected for that lens mass. Figure 9 shows this generic distribution for lenses of $1M_\odot$ mass, changing with M_L by simply scaling the abscissa with $\sqrt{M_L/M_\odot}$. It has been established by assuming that the lenses are spatially distributed according to the so-called standard dark matter halo model described in Blaineau et al. (2022). Table 2 shows, for a series of lens masses, the maximum expected fractions of situations where binaries could affect microlensing detection, splitted into 3 domains of projected Einstein radius R_E/x . For each lens mass, the event fraction for each domain is deduced from the distribution of Fig. 9 properly scaled. For $R_E/x < 50AU$, we conservatively assume that 100%

| $M_L (M_\odot)$ | 1 | 3 | 10 | 30 | 100 |
|---------------------|------|------|------|------|------|
| $R_E/x < 50AU$ | 71% | 34% | 9% | 2% | 0.4% |
| max. contribution | 71% | 34% | 9% | 2% | 0.4% |
| $50 < R_E/x < 1000$ | 29% | 66% | 91% | 97% | 95% |
| max. contribution | 1.8% | 3.9% | 4.6% | 4.0% | 4.8% |
| $R_E/x > 1000AU$ | 0% | 0% | 0.2% | 0.8% | 5% |
| max. contribution | 0% | 0% | 0% | 0% | 0.1% |
| Total | 73% | 38% | 14% | 6.2% | 5.3% |

Table 2: Fractions of events toward LMC within the 3 domains of projected Einstein radius, and their maximum contributions to the fraction of events with significant blending due to binarity.

of the events can be affected by blending due to binarity; for $50AU < R_E/x < 1000AU$, we integrate the most pessimistic function of Fig. 8, weighted by the normalised distribution of R_E/x ; for $R_E/x > 1000AU$, we consider that a maximum of 2% of the events can be affected by blending due to binarity.

The total given in the table is the maximum proportion of events for which the classical detection efficiency calculation is not applicable, because of the additional risk of event superposition or blend due to the binarity of the sources. In the absence of a specific simulation, the status of these events on binaries in terms of detection efficiency is poorly known, and this must be taken into account as a systematic uncertainty for the measurement of optical depths and event rates.

This study shows that the impact of source binarity can be neglected to first order when searching for gravitational microlensing effects from lenses heavier than $30M_\odot$. The maximum value of uncertainty 6.2% is all the smaller as the lenses are massive (Fig. 9), showing that binarity of LMC sources must have an additional effect to the estimates of accidental blending effects that can be neglected for heavy lenses, as was done in Blaineau et al. (2022). Figures 8 and 9 allows to estimate these numbers in case of even more massive lenses towards the LMC. For an estimate corresponding to another Galactic halo model, or to other targets than LMC, Fig. 9 needs to be rebuild.

For events due to lighter lenses with a larger probability of projected Einstein radii $R_E/x < 50AU$, it is currently not possible to draw reliable conclusions on the impact of the blend due to the binarity of the LMC sources with our technique. An alternative method for estimating the differential binarity rate with a projected separation of less than 50AU is needed, coupled with a specific simulation to estimate the detection efficiency of non-PSPL events.

8.2. Discussion on stellar populations

Since the majority of the stars observed in the LMC correspond to the brightest stars in the Gaia data that we use (Fig. 4), we investigated the variation of the binarity rate $F_{bin}(200AU)$ with the magnitude of the stars. We therefore reproduced our analysis by restricting our sample to two absolute magnitude g domains, between -0.5 and 4.5 mag (3,090,000 stars) and between 4.5 and 9.5 mag (612,000 stars), always limiting the maximum difference in magnitudes between the two components to 2.5. The statistical power here is significantly reduced for the population with $-0.5 < g < 4.5$, but we nevertheless find a significantly lower binarity rate for bright star pairs ($F_{bin}(200AU) = 1.42 + / - 0.08\%$) than for faint star pairs ($F_{bin}(200AU) = 2.58 + / - 0.04\%$). It is therefore likely that

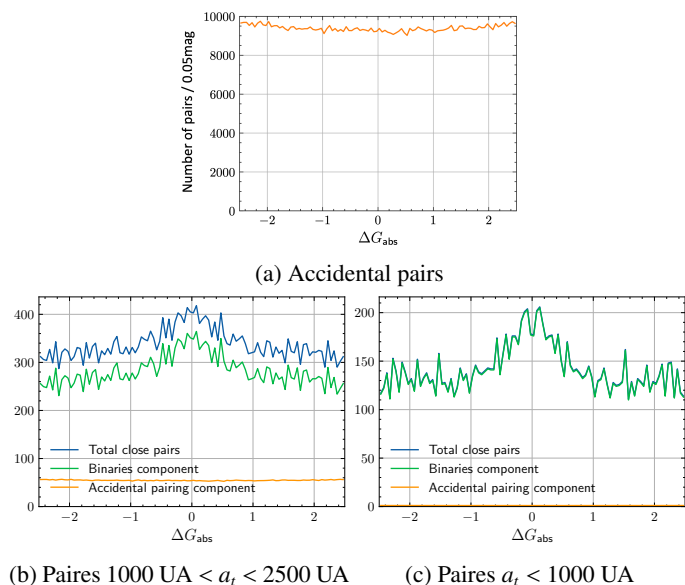


Fig. 10: Distribution of magnitude differences between the stars of pairs, in pairs per 0.05 magnitude interval. Figure (a) shows distribution of magnitude differences between stars separated by more than $30000UA$ (only due to fortuitous alignments). Figures (b) and (c) show in blue the same distributions for pairs separated by less than 2500 et $1000 UA$, in orange the distributions for the fortuitous alignments, normalised according to the sample size, in green the difference between the two distributions (*i.e.* the distribution of magnitude difference for binary systems only). These figures have one entry per star. In figure (c) the number of fortuitous alignments is negligible, then the orange distribution is almost zero, and green and blue distributions are superimposed.

in LMC catalogs like the EROS2 or MACHO surveys, which are composed of rather bright stars, we overestimate the binarity rate by assuming that the stellar populations from our Gaia sample and in the LMC are similar.

We also investigated whether there are correlations between magnitude differences and the separation a_t of binaries. Figure 10 shows the distributions of magnitude differences ΔG between components for binaries with $1000UA < a_t < 2500UA$ (Fig. 10(b)) and with $a_t < 1000UA$ (Fig. 10(c)), obtained by subtracting from the observed distributions the expected distributions for random pairs (Fig. 10(a)), with appropriate normalization. The latter distribution is deduced from that of the difference ΔG of pairs separated by $a_t > 30000AU$ — which turns out to be approximately uniform —. It appears that the closer the binary system, the smaller the difference in magnitude between components. It is tempting to explain this difference by the intervention of a gravitational capture mechanism, which would favor the formation of distant binaries, whose luminosities would be consequently less correlated. These observations are corroborated by the distribution of mass ratios as a function of the semi-major axis or period of the binary systems in Moe & Di Stefano (2017).

Finally, we examined the case of red giants, which constitute an important part of the catalogs of the historical microlensing surveys to the LMC. Unfortunately, they represent too few stars in our Gaia sample to establish a reliable binarity rate. However, we examined the magnitude distribution of stars in pairs with separation $a_t < 2500UA$ containing at least one giant. In this sample of pairs, we found that there are almost no giant

binary systems (less than 1% of the sample), but only binaries consisting of a giant and a main sequence star, with magnitude difference ΔG smaller than 2.5 in 85% of the cases. This fact reinforces our conclusion that we probably overestimate the proportion of binaries in EROS2/MACHO type catalogs by extrapolating the binarity rate measured in Section 7.

9. Conclusions: The impact of binarity on microlensing surveys

We conclude from this study that the search detection efficiency of long duration microlensing events due to lenses heavier than $30M_\odot$ toward LMC is not significantly affected by the source binarity. This result is useful not only in the recent combined analysis of EROS and MACHO data spanning several decades (Blaineau et al. 2022), but also in future research with Rubin-LSST.

On the other hand, for lenses lighter than $30M_\odot$, as soon as the projected Einstein radius is less than a few tens of AU , the binarity rates extrapolated here are higher and less reliable. The fraction of events that can be affected by blending due to source binarity becomes less negligible, and another study must be undertaken to estimate the impact of a binarity rate that may be high (but probably positive) on the detection efficiency.

Although it is not possible to estimate from the Gaia database the differential binarity rate for $a_t < 50AU$ in the LMC, one can conversely consider detecting binarity effects by measuring distortions with respect to a simple (PSPL) microlensing effect. In particular, if the photometric accuracy of LSST reaches a few milli-magnitudes, one could use possible deviations from PSPL microlensing effects to infer source binarity rates.

Our study of the impact of binarity rates on microlensing detection efficiency toward the LMC is easily transferable, through some scaling and modelisation of the lens spatial distribution, to studies of microlensing within the Galactic plane. In this case, the source population should better resemble the one studied in this paper. Our last comment is that the use of a tolerant pre-filtering, not sensitive to the precise shape of the magnification curve, remains the safest technique to mitigate the effects of distortion due to the binarity of the source on the detection efficiency.

Acknowledgements. We thank Olivier Perdereau for his useful comments on the manuscript. This work was supported by the Paris Ile-de-France Region.

References

- Alcock, C., Akerlof, C., Allsman, R., et al. 1993, *Nature*, 365
- Aubourg, E., Bareyre, P., Bréhin, S., et al. 1993, *Nature*, 365, 623
- Bertin, E. & Arnouts, S. 1996, *A&AS*, 117, 393
- Blaineau, T. 2021, PhD thesis
- Blaineau, T. & Moniez, M. 2020, *A&A*, 636, L9
- Blaineau, T., Moniez, M., Afonso, C., et al. 2022, *A&A*, 664, A106
- Dhital, S., West, A. A., Stassun, K. G., & Bochanski, J. J. 2010, *The Astronomical Journal*, 139, 2566
- Duchêne, G. & Kraus, A. 2013, *Annual Review of Astronomy and Astrophysics*, 51, 269
- Duquenooy, A. & Mayor, M. 1991, *A&A*, 500, 337
- Fabricsius, C., Luri, X., Arenou, F., et al. 2020, arXiv e-prints, arXiv:2012.06242
- Gaia Collaboration, Brown, A. G. A., Vallenari, A., et al. 2020, arXiv e-prints, arXiv:2012.01533
- Gaia Collaboration, Prusti, T., de Bruijne, J. H. J., et al. 2016, *A&A*, 595, A1
- Griest, K. 1991, *ApJ*, 366, 412
- Griest, K. & Hu, W. 1992, *ApJ*, 397, 362
- HST archive. 2002, <https://archive.stsci.edu/>
- Landy, S. D. & Szalay, A. S. 1993, *ApJ*, 412, 64
- Lindgren, L., Klioner, S. A., Hernández, J., et al. 2021, *A&A*, 649, A2

- Lindgren, L., Lammers, U., Hobbs, D., et al. 2012, *A&A*, 538, A78
Luri, X., Brown, A. G. A., Sarro, L. M., et al. 2018, *A&A*, 616, A9
Moe, M. & Di Stefano, R. 2017, *ApJS*, 230, 15
Mróz, P., Udalski, A., Skowron, J., et al. 2019, *ApJS*, 244, 29
Paczynski, B. 1986, *ApJ*, 304, 1
Raghavan, D., McAlister, H. A., Henry, T. J., et al. 2010, *ApJS*, 190, 1
Rahvar, S. 2015, *International Journal of Modern Physics D*, 24, 1530020
Schneider, P., Kochanek, C., & Wambsganss, J. 2006, *Gravitational Lensing: Strong, Weak and Micro*
Tisserand, P., Le Guillou, L., Afonso, C., et al. 2007, *A&A*, 469, 387
Udalski, A., Szymanski, M., Kaluzny, J., et al. 1993, *Acta Astron.*, 43, 289
Wyrzykowski, L., Skowron, J., Kozłowski, S., et al. 2011, *MNRAS*, 416, 2949
Zavada, P. & Piška, K. 2020, *AJ*, 159, 33